

Single-nucleus RNA sequencing resolves microenvironmental dynamics in brown/beige adipose tissue after bariatric surgery

Received: 5 July 2025

Accepted: 11 November 2025

Published online: 22 December 2025

Cite this article as: Wang W., Wang Y., Guo Z. *et al.* Single-nucleus RNA sequencing resolves microenvironmental dynamics in brown/beige adipose tissue after bariatric surgery. *J Transl Med* (2025). <https://doi.org/10.1186/s12967-025-07480-5>

Wei Wang, Yangxinyun Wang, Zhonghao Guo, Yao Lu, Wei Xie & Ruibin Li

We are providing an unedited version of this manuscript to give early access to its findings. Before final publication, the manuscript will undergo further editing. Please note there may be errors present which affect the content, and all legal disclaimers apply.

If this paper is publishing under a Transparent Peer Review model then Peer Review reports will publish with the final article.

Single-nucleus RNA sequencing Resolves Microenvironmental Dynamics in Brown/Beige Adipose Tissue after Bariatric Surgery

Wei Wang¹, Yangxinyun Wang², Zhonghao Guo², Yao Lu¹, Wei Xie^{3*}, Ruibin Li^{2*}S

¹ Department of Endocrinology, First Affiliated Hospital of Baotou Medical College, Baotou, Inner Mongolia 014010, China

² Daytime surgery center, First Affiliated Hospital of Baotou Medical College, Baotou, Inner Mongolia 014010, China

³ Department of Medical Technology and Anesthesia, Baotou Medical College, Baotou, Inner Mongolia 014010, China

*Correspondence Author: Ruibin Li, 15849472388@163.com; Wei Xie: xiewei@tmu.edu.cn

Abstract

Background

Obesity is a chronic condition characterized by excessive adipose tissue accumulation, which significantly contributes to a range of systemic comorbidities, including type 2 diabetes, cardiovascular diseases, and various forms of cancer. These associated health issues severely compromise individuals' quality of life and pose substantial challenges for public health. Despite the known benefits of bariatric surgery as the most effective intervention for achieving sustained weight loss and improving metabolic profiles, the underlying biological mechanisms that facilitate adipose tissue remodeling following surgical intervention remain inadequately understood.

Methods

In this study, we employed single-nucleus RNA sequencing to construct high-resolution transcriptional maps of murine brown adipose tissue (BAT) and beige adipose tissue both before and after bariatric surgery. This comprehensive analysis allowed us to explore dynamic changes in the adipose tissue microenvironment post-surgery.

Results

Our findings revealed a significant post-surgical expansion of fibroblastoid (FBO) populations in both BAT and beige adipose tissues. This expansion was accompanied by a marked reduction in adipocytes (AP). To further understand the cellular interactions underlying these changes, cell communication analysis was conducted through the CellChat platform. This analysis indicated enhanced crosstalk between adipocytes and fibroblastoid cells, predominantly mediated by IGF1 signaling activation. In contrast, interactions involving the VEGF pathway between adipocytes and endothelial cells (EC) were suppressed. Moreover, pseudotemporal trajectory analysis identified a distinct subpopulation of adipocytes, termed AP6, that was enriched for fibrosis-associated genes and showed progressive upregulation of 11 genes along differentiation toward fibroblastoid states.

Conclusion

We delineate post-bariatric microenvironmental reprogramming in thermogenic adipose depots and highlight a candidate pathway in which 11 putative transition regulators cooperate with IGF1 signaling to promote AP6-cell transdifferentiation toward fibroblastoid lineages. These data nominate testable targets for therapeutic modulation of obesity and its complications. Given the limited sample size, findings are descriptive and hypothesis-generating; definitive lineage inference awaits validation by fate mapping or RNA-velocity in larger cohorts.

Keywords

Obesity; Bariatric surgery; Single-nucleus RNA sequencing; Fibroblastoid; Adipocytes

Introduction

Overweight and obesity, characterized by abnormal or excessive adipose tissue accumulation that presents significant health risks, are defined by a body mass index (BMI) exceeding 25 kg/m² (overweight) and 30 kg/m² (obesity)[1]. In 2017, elevated BMI contributed to an estimated 4.7 million deaths from non-communicable diseases, underscoring its global health burden[2]. The World Obesity Federation's 2025 Report projects that over 2.9 billion adults worldwide will be affected by high BMI by 2030, cementing obesity as a pressing public health challenge[3]. While lifestyle interventions targeting diet and physical activity remain first-line treatments, their long-term efficacy is often limited. Currently, bariatric surgery stands as the most effective therapeutic option for sustained weight loss and mitigation of obesity-related comorbidities[4]. This procedure induces anatomical and physiological remodeling of the gastrointestinal tract, reducing gastric capacity and modulating gut-brain axis signaling through altered hormone secretion, thereby promoting satiety and suppressing appetite[5-7]. Post-surgical weight loss drives significant structural and metabolic adaptations in adipose tissue, which in obesity exhibits pathological features such as chronic inflammation and fibrosis[8]. However, the molecular and cellular dynamics underlying adipocyte remodeling before and after surgical intervention remain incompletely elucidated.

Adipose tissue exists in three histologically distinct forms: white (WAT), brown (BAT), and beige. WAT serves as the primary energy storage depot and metabolic regulator, whereas brown adipose tissue (BAT) specializes in thermogenesis through uncoupled mitochondrial respiration, dissipating energy as heat. Beige adipocytes, a plastic intermediary phenotype embedded within WAT, can adopt BAT-like characteristics—including multilocular lipid droplets and elevated mitochondrial density—under stimuli such as cold exposure or β -adrenergic signaling[9-12]. This thermogenic capacity positions BAT and beige adipose tissue as promising therapeutic targets for enhancing systemic energy expenditure in metabolic disorders[13-15]. Recent single-nucleus RNA sequencing (snRNA-seq) studies of WAT in murine models have revealed an "obesogenic memory" encoded at the epigenetic level, wherein adipocytes retain molecular signatures of prior metabolic stress that predispose to weight regain[16]. Additionally, excessive interstitial fibrosis in WAT, driven by chronic inflammation, may mechanically constrain adipocyte shrinkage during weight loss[17-19]. Despite these advances, the cellular and molecular landscapes of BAT and beige adipose plasticity following bariatric surgery remain unexplored at **single-nucleus resolution**.

Given that mature adipocytes are too large and fragile for traditional single-cell methods, single-nucleus RNA sequencing (snRNA-seq) enables the profiling of all cell types within adipose tissue, including these otherwise intractable adipocytes[20-22]. This study leverages snRNA-seq datasets to systematically map the spatiotemporal reorganization of brown and beige adipose tissue microenvironments before and after bariatric surgery. We interrogate dynamic shifts in intercellular communication networks, identify key signaling pathways governing post-surgical adipose remodeling, and delineate core transcriptional regulators driving these adaptations. Through integrative multi-omics analyses – including ligand-receptor interaction mapping, pseudotemporal trajectory reconstruction, and pathway enrichment—we unveil the mechanistic interplay between thermogenic adipose subtypes and surgical weight loss. Our findings provide a high-resolution atlas of adipose tissue plasticity, offering insights into therapeutic strategies to sustain metabolic benefits post-intervention.

Methods

Experimental animals and grouping

Four-week-old male C57BL/6J mice were housed at $22 \pm 2^\circ\text{C}$ under a 12-h light/12-h dark cycle. At 4 weeks of age, animals were switched to a high-fat diet (HFD; 60 % kcal from fat). After 16 weeks of HFD exposure (i.e., at 20 weeks of age), mice were randomly allocated to two intervention groups: sham-operated (Sham) or sleeve gastrectomy (SG). All procedures were performed at 20 weeks of age, and mice were euthanized 4 weeks later (24 weeks of age). Animal protocols were approved by the Medical Ethics Committee of the First Affiliated Hospital of Baotou Medical College, Inner Mongolia University of Science and Technology (approval no. 2024D027).

Surgical protocol and postoperative care

Pre-operative preparation and anaesthesia: Mice were fasted for 12 h and deprived of water 1 h before surgery. General anaesthesia was induced with 2-3 % isoflurane in O_2 ($2-3 \text{ L min}^{-1}$) and maintained at $0.8-1.5 \text{ L min}^{-1}$. Body temperature was kept at 35°C with a heating pad. Following fur clipping and iodophor disinfection, a sterile surgical field was established. To prevent intra-operative dehydration, 1 mL sterile saline was administered subcutaneously.

Sleeve gastrectomy: A 4-cm midline laparotomy was performed below the xiphoid process. The stomach was exteriorized with cotton swabs and forceps. The hepatogastric ligament, gastrosplenic ligament, short gastric vessels, and gastroepiploic vessels adjacent to the antrum were cauterised with micro-electrocautery. Two micro-vascular clamps were applied: one 2-3 mm below the gastro-oesophageal junction and the other on the anterior gastric wall ~ 5 mm proximal to the pylorus along the greater curvature. Approximately 80 % of the gastric greater curvature, including the entire fundus, was resected with micro-scissors along the outer edge of the clamps. Gastric contents were removed and the remnant stomach was disinfected with

iodophor. The gastric incision was closed with continuous 6-0 sterile silk sutures, returned to the abdominal cavity, and the laparotomy was closed in layers after thorough irrigation and disinfection.

Sham operation: Sham mice underwent identical anaesthesia, laparotomy, and stomach mobilisation without resection.

Postoperative care: On postoperative day (POD) 1, mice were kept on a heating pad to prevent hypothermia. Meloxicam (2 mg kg^{-1} s.c.) was administered once daily for analgesia on POD 1-3. POD 1: fasting with isotonic glucose-saline (0.2 mL every 4 – 6 h). POD 2-3: liquid diet; POD 4-6: soft HFD; POD 7: return to standard HFD to ensure secure healing of the gastric incision.

Adipose-tissue collection: At 24 weeks of age (4 weeks post-surgery), mice were euthanized. Beige adipose tissue was isolated from the distal portion of the mouse inguinal fat pad, and brown adipose tissue was obtained from the interscapular region between the two scapulae on the mouse’s back. Tissues were rinsed in ice-cold RNase-free PBS, blotted dry, snap-frozen in liquid nitrogen, and stored at -80°C until downstream sequencing. For each sequencing sample, adipose tissue from three mice was pooled.

snRNA-seq Analysis

Batch correction and data integration: Batch correction was performed to mitigate non-biological variations arising from multi-batch or multi-platform data integration. Using the FindIntegrationAnchors function in the Seurat package (v4.4.0), shared biological variation across batches was identified via canonical correlation analysis (CCA). Anchors—cell pairs with cross-batch biological consistency—were determined in the reduced-dimensional CCA space. Technical biases were quantified by anchor pairwise differences and corrected through a mutual nearest neighbors (MNN)-based non-linear transformation.

Dimensionality reduction and clustering: Gene expression matrices were normalized (NormalizeData), scaled (ScaleData), and filtered for the top 2,000 variable genes (FindVariableFeatures) according to the published study[23]. Principal component analysis (PCA) was applied to the scaled data (RunPCA), followed by uniform manifold approximation and projection (UMAP) using the first 30 principal components (RunUMAP). Cell clusters were identified (FindClusters, resolution = 0.8) based on a shared nearest neighbor graph constructed from the PCA embeddings (FindNeighbors).

Pathway activity scoring via AUCell: Adipose-related pathway activities were quantified at **single-nucleus resolution** using AUCell. Genes within each cell were ranked by expression, and the area under the curve (AUC) for cumulative distributions of predefined gene sets was computed. Scores were stored as an assay in the Seurat object and visualized via Dotplot to compare pathway activities across cell types.

Intercellular communication analysis with CellChat: CellChat (v1.6.0) inferred ligand-receptor-mediated communication networks by integrating expression data with a curated interaction database. Interaction weights were derived from ligand/receptor co-expression and pathway hierarchy. Network significance was assessed using permutation tests (1,000 iterations), and the Trimean-L/R model quantified signal transmission strength. Secreted signaling networks centered on adipocytes were analyzed to elucidate adipocyte-microenvironment crosstalk. By assigning a cell communication probability value to each interaction and conducting permutation tests, we inferred biologically meaningful cell-cell communication.

Gene set variation analysis (GSVA): The GSVA R package (v1.48.0) evaluated enrichment scores for IGF- and VEGF-related pathways across cell types. This non-parametric method identified gene sets with significant expression variation by comparing their ranked expression profiles to a background model.

Pseudotime trajectory inference using Monocle2: Cell differentiation trajectories were reconstructed with Monocle2 (v2.26.0). After dimensionality reduction via DDRTree, a minimum spanning tree (MST) was constructed to order cells along pseudotime. Branch points and dynamic gene expression patterns were identified to delineate AP differentiation into fibroblastoid (FBO) and characterize AP subpopulation trajectories.

Candidate transition regulator selection: Primary filters: 1) FBO%/AP*% > 2; 2) EC%/AP*% < 0.8 (to reduce the likelihood of endothelial transdifferentiation.); Secondary filters: 1) AP* expression $\geq 15\%$ of cells; 2) FBO%/AP*% > 3. These criteria enrich for genes that are not merely markers but potential drivers of AP* → FBO conversion. Here, AP* denotes the adipocyte subcluster that lies closest to FBO in the trajectory analysis described above.

Statistical analysis and visualization: All analyses were executed in R (v4.3.2) using Seurat, AUCell, CellChat, GSVA, and Monocle2. Figures were generated with ggplot2 and Seurat's visualization utilities.

Immunofluorescence

OCT-embedded, 10 μm adipose cryosections (4% PFA, 4°C, 12h) were blocked (0.3% PBST + 5% BSA, 30min, RT) and subjected to two sequential antibody panels. Panel 1: Rabbit anti-Neb1 (1:500, 21497-1-AP, Proteintech) → AF488 donkey anti-rabbit (1:1,000, A-21206, Invitrogen); citrate retrieval; goat anti-Igf1r (1:500, AF-305-SP, R&D Systems) → AF647 donkey anti-goat (1:500, A-21447, Invitrogen); retrieval; PE-anti-Nucb2 (1:300, orb491174, Biorbyt). Panel 2: Rat anti-Emcn (1:100, ab106100, Abcam) → AF488 donkey anti-rat (1:1,000); rabbit anti-Vegfa (1:300, ab52917, Abcam) → AF647 donkey anti-rabbit (1:1000, A-31571, Invitrogen); PE-anti-Nucb2 (1:300, orb491174, Biorbyt). All incubations: primary 4°C overnight; secondary 37°C 1h, dark. Nuclei stained with DAPI; slides mounted in antifade medium. Images acquired under identical microscope settings.

Results

Dynamic Changes in Brown and Beige Adipose Tissue After Bariatric Surgery

After rigorous quality control and filtering of snRNA-seq data from adipose tissue of bariatric surgery and sham-operated mice (Table 1, Supplementary Table1, Supplementary Figure 1), we retained 34,772 high-quality nuclei. Subsequent batch correction and mapping of samples onto a UMAP 2D space (Fig. 1A) confirmed the absence of significant batch effects. Leveraging published adipose tissue marker genes[24-30], we identified 12 major cell types: B cell, adipocyte (AP), macrophage (MP), NK cell, T cell, endothelial cell (EC), monocyte (Mono), myeloid dendritic cell (mDC), fibroblast (FB), muscle cell (muscle), and smooth muscle cell (SMC). A distinct cell subset with high expression of *Neb1* and *Mylk* (canonical myoFB markers) but lacking the broader fibroblast gene signature; therefore, we designate it as fibroblastoid (FBO) (Fig. 1B). To authenticate the annotation accuracy, we examined the expression of known marker genes across cell types. As depicted in Fig. 1C, the annotated cell types exhibited specific marker gene expression, thereby validating our annotation precision.

To delineate alterations in the adipose tissue microenvironment, we quantified the proportion of each cell type within samples (Fig. 1D). The analysis revealed a decline in adipocyte, NK cell, and EC proportions concomitant with a rise in FBO proportion, underscoring a post-surgical shift in the cellular microenvironment. At the pathway level, we observed that in brown adipose tissue, pathways negatively regulating brown fat cell differentiation exhibited attenuated activity post-surgery (Fig. 1E). Similarly, in beige adipose tissue, adipocyte-related pathways were downregulated post-surgery (Fig. 1F), with fat storage pathways suppressed and free fatty acid release pathways activated, (such as WANG-CLASSIC-ADIPOGENIC-TARGETS-OF-PPARG pathway in Fig. 1F) potentially supplying energy to brown fat or other tissues such as muscle. Collectively, these findings demonstrate that bariatric surgery induces significant remodeling of the brown and beige tissue microenvironments, reducing adipocyte proportions and modulating adipocyte pathway activities.

Table 1. Samples for snRNA-seq

Sample ID	Groups	Type
Je	Sham	BAT
Ji	Sham	Beige
Se	Surgery	BAT
Si	Surgery	Beige

Fig. 1 Single-nucleus atlas uncovers postoperative cellular dynamics in adipose tissue

(A) UMAP projection of nuclei, with colors representing different samples (Je, n = 10111; Ji, n = 10027; Se, n = 8838; Si, n = 5796); (B) UMAP projection of nuclei, with colors representing different cell types (AP, n = 10363; B, n = 2303; mDC, n = 204; EC, n = 4833; FB, n = 4018; MP, n = 3550; Mono, n = 110; muscle, n = 265; NK, n = 472; FBO, n = 4858; SMC, n = 835; T, n = 1930; Unknown, n = 1030); (C) Bubble plot visualization of cell type-specific marker gene expression. Darker shades denote higher average expression levels within each annotated cell type, while bubble size reflects the percentage of cells in that subtype expressing the given marker gene; (D) Stacked-bar comparison of cell-type proportions across samples, with colors coding for the annotated cell types; (E) Brown adipose tissue pathway activity. Top 5 |logFC| pathways are shown; dot size = fraction of cells with high activity, color intensity = mean activity level; (F) Beige adipose tissue pathway activity. Top 5 |logFC| pathways are shown.

Adipocyte Interaction

To elucidate adipocyte interactions within the microenvironment, we analyzed cellular interactions in adipose tissue with a focus on AP, FBO, and EC, which exhibited substantial proportional changes post-surgery. The complete list of significantly altered pairs is provided in [Supplementary Table 2](#). In brown adipose tissue, regardless of whether AP acted as signaling or target cells, the interaction strength between AP and FBO increased, whereas that between AP and EC decreased ([Fig. 2A](#)). Differential receptor-ligand analysis revealed weakened AP-EC interactions, evidenced by reduced interactions of Vegfb-Vegfr1, Vegfa-(Vegfr2, Vegfr1), Retn-Tlr4, Igf1-Igf1r, Angptl4-Cdh5, Angptl-Tek, Adipoq-Adipor2, and Bmp6-(Bmpr1a + Bmpr2, Bmpr1a + Acvr2a, Acvr1 + Bmpr2, Acvr1 + Acvr2a). Post-bariatric surgery, the most pronounced reduction was observed in Vegf-related receptor-ligand pairs, with a high probability of communication. Conversely, AP-FBO interactions were enhanced, accompanied by strengthened Igf1-Igf1r, Sema3c-(Nrp1 + Plxna2), Nampt-Insr, Gas6-Mertk, Fgf2-Fgfr2, and Adipoq-Adipor2 interactions, among which Igf1-Igf1r exhibited the highest communication probability ([Fig. 2B](#)).

In beige adipose tissue, the interaction strength between AP and FBO increased irrespective of AP's role, mirroring findings in brown adipose tissue. However, when AP acted as a

signaling cell, its interaction with EC intensified, whereas as a target cell, this interaction weakened (Fig. 2C), diverging from observations in brown adipose tissue. Further examination of differential receptor-ligand pairs revealed, consistent with brown adipose tissue, enhanced Igf1-Igf1r and Nrg2-ErbB4 interactions during strengthened AP-FBO interactions, with Igf1-Igf1r communication probability surpassing that of Nrg2-ErbB4. These results collectively indicate that post-surgery, AP-FBO interactions are augmented, coinciding with enhanced Igf1-Igf1r receptor-ligand interactions (Fig. 2D).

Fig. 2 Adipocyte-centric interactions after surgery (**A, B**) Differential signaling networks centred on AP cells. Left: AP as the signaling cell; right: AP as the target cell. Red edges = up-regulated interactions in Se vs. Je; blue edges = down-regulated interactions in Se vs. Je; edge width = magnitude of change, Brown adipose tissue (**A**), Beige adipose tissue (**B**); (**C, D**) Top-ranked receptor–ligand pairs identified by cell communication analysis. Brown adipose tissue (**C**), Beige adipose tissue (**D**)

Postoperative Alterations in IGF/VEGF Pathways

Given the receptor-ligand interaction changes involving the IGF1 and VEGF pathways, we conducted a GSVA analysis to delineate pre- and post-surgery pathway activity dynamics. The analysis revealed that post-surgery, FBO in both brown and beige adipose tissues exhibited elevated IGF1 pathway activity (Fig. 3A–B), while EC in these tissues demonstrated suppressed VEGF pathway activity (Fig. 3C–D). When integrated with cellular interaction data, these findings suggest that enhanced AP-FBO interactions may correspond to upregulated IGF1 pathway activity, whereas weakened AP-EC interactions might correlate with diminished VEGF pathway activity.

Fig. 3 Postoperative rewiring of IGF/VEGF signaling Heat-maps of pathway-activity scores (Je vs Se) for (A) brown-adipose FBO, (B) beige-adipose FBO, (C) brown-adipose EC, and (D) beige-adipose EC. Red = higher average activity; blue = lower activity

Pseudotime Trajectory Analysis of AP-FBO Transition

To delve deeper into the implications of strengthened AP-FBO interactions in brown adipose tissue, we performed a pseudotime trajectory analysis to investigate the potential transition of AP to FBO. After batch correction, brown adipose tissue samples containing AP and FBO were mapped onto a UMAP 2D space, confirming the absence of significant batch effects (Fig. 4A). Subsequent dimensionality reduction and clustering of the top 2,000 variable genes at a resolution of 0.3 (Fig. 4B) enabled the sub-clustering of brown adipose tissue adipocytes into eight subtypes (AP0-AP7). Mapping these adipocyte subtypes onto the AP- and FBO-clustered UMAP revealed the transitional AP6 subtype in proximity to FBO (Fig. 4C). Monocle2-based trajectory analysis of brown adipose tissue AP and FBO cells consistent with a potential transition of AP cells toward FBO (Fig. 4D). Furthermore, cell-type-based trajectory analysis uncovered a continuous transition trajectory: AP7-AP4-AP0-AP5-AP1-AP2-AP3-AP6-FBO (Fig. 4E).

Fig. 4 Pseudotemporal reconstruction of the AP-to-FBO transition in brown adipose tissue (A) UMAP of AP and FBO cells colored by sample origin; (B) Same embedding colored by

subcluster; (C) Subcluster identity annotation for (B); (D) Monocle2 trajectory branching across different conditions with pseudotime progression from AP (root) to FBO (terminus); (E) Trajectory plot colored by cell type illustrating the continuum of transition

Pseudotime Trajectory Analysis of AP Cell Transition

To explore the mechanism underlying AP-to-FBO transition in brown adipose tissue, we conducted trajectory analysis of the eight AP subtypes. The results revealed a cell trajectory: AP3, AP4, AP5, AP7-AP0-AP1-AP2-AP6 (Fig. 5A). Subsequent branch-specific gene clustering at node 3 identified *Zbtb16*, *Fam13a*, *Gm26917*, *Fkbp5*, and *Dcun1d3* as genes exhibiting upregulated expression along this trajectory (Fig. 5B). Among these, *Zbtb16*, *Fam13a*, and *Fkbp5* have been confirmed to participate in fibrosis promotion[31-33], thereby reinforcing the plausibility of AP-to-FBO transition.

Fig. 5 Pseudotemporal ordering of AP subcluster transitions (A) Monocle2 trajectory of brown-adipose AP cells colored by subcluster; node 3 marks the root; (B) Branch-specific gene modules. Pre-branch: cells mapping from node 3 toward pseudotime 0 (AP0, AP3, AP4, AP5, AP7). Fate 1: cells extending from node 3 to lower-ID branches (AP1, AP2). Fate 2: cells extending from node 3 to higher-ID branches (AP6). (AP0, n = 1907; AP1, n = 1039; AP2, n = 1015; AP3, n = 561; AP4, n = 91; AP5, n = 57; AP6, n = 45; AP7, n = 42)

Key Potential Regulators of AP-FBO Transition

In our quest to identify key regulators of AP-to-FBO transition, we first identified differentially expressed genes between brown adipose tissue adipocyte subtype AP6 and other

AP subtypes, uncovering 741 upregulated and 5,198 downregulated genes ($\text{FDR} < 0.05$, $|\log\text{FC}| > 0.5$; Fig. 6A, Supplementary Table 3). Focusing on these up-regulated genes, we next screened for candidate regulators (see Methods) and identified 11 potential key genes (Fig. 6B): *Rims2*, *Cacna2d3*, *Parp8*, *St8sia6*, *Enah*, *Nucb2*, *Nexmif*, *Iqgap2*, *Dtnb*, *Ano1*, and *Ptpn22*.

Among these genes, we first investigated *Nucb2* for its literature relevance with lipid regulation. Nesfatin-1, encoded in the nucleobindin-2 (*Nucb2*), is widely distributed in brain nuclei and functional cells[34]. Nesfatin-1 is a pivotal molecule regulating brown adipocyte differentiation and triglyceride utilization[35] and plays a crucial role in lipid homeostasis regulation. Additionally, Nesfatin-1 has been reported to regulate feeding, glucose, and fat metabolism, thereby maintaining energy balance through sympathetic nervous system-mediated peripheral fat metabolism regulation[36, 37]. Spatial mapping revealed specific high expression of *Nucb2* in AP6 (Fig. 6C). Co-expression analysis of *Nucb2* with *Igflr* in brown adipose tissue FBO indicated that 7.8% expressed only *Nucb2*, 38.9% only *Igflr*, and 44.5% co-expressed both, suggesting a tendency for co-expression of *Nucb2* and *Igflr* in brown adipose tissue FBO (Fig. 6D, 6F). In addition to *Nucb2*, we also performed co-expression analysis on the aforementioned 10 other genes. We also observed their co-expression with *Igflr* in FBOs (Supplementary Figure 2). On the other hand, in EC, 14.9% expressed only *Nucb2*, 3.1% only *Vegfa*, and 2.0% co-expressed both, indicating mutually exclusive expression of *Nucb2* and *Vegfa* (Fig. 6E, 6G). These results collectively suggest that these 11 genes may facilitate AP-to-FBO transition through activating the IGF1 pathway.

To identify beige-adipocyte equivalents of BAT-AP6, we first defined the AP6 signature as genes with adjusted p -value ($\text{adj. } p < 0.05$) and log₂ fold change ($\log_2\text{FC} > 0.5$) versus other BAT-AP clusters (Supplementary Table 4). Among beige-adipocyte clusters, cluster 4 showed the highest transcriptional overlap (Supplementary Fig. 3A–B). Applying the same cut-offs, *Parp8* and *Fyb* surfaced as potential AP→FBO transition genes; *Parp8*, also a top hit in BAT (Supplementary Fig. 3C–D), will be functionally validated in follow-up studies.

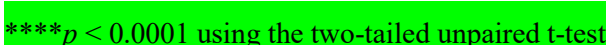
Fig. 6 *Nucb2* as a potential AP-to-FBO transition gene **(A)** Volcano plot of genes expressed in AP6 versus all other AP subclusters (brown adipose tissue); **(B)** Candidate transition genes enriched in AP6; **(C)** *Nucb2* expression distribution across AP subclusters; **(D)** Relative abundance of FBO subsets defined by *Nucb2/Igf1r* co-expression: *Nucb2⁺Igf1r⁻*, *Nucb2⁺Igf1r⁺*, *Nucb2⁻Igf1r⁻*, *Nucb2⁻Igf1r⁺*; **(E)** Same as **(D)** for EC populations; **(F)** Correlation between *Nucb2* and *Igf1r* gene levels within FBO; **(G)** Correlation between *Nucb2* and *Vegfa* gene levels within EC

Cross-species validation of adipose microenvironment remodeling after Bariatric Surgery

To functionally corroborate the snRNA-seq predictions, we performed multiplex immunofluorescence on mouse BAT. Consistent with the transcriptional atlas, Se mice displayed a significantly lower abundance of *Emcn*⁺ ECs ([Supplementary Fig. 4A](#)) and a markedly higher density of *Nebl*⁺ FBOs ([Supplementary Fig. 4B](#)) than Je controls ([Fig. 7A](#)). *Vegfa* signal intensity was reduced in Se ECs ([Supplementary Fig. 4C](#)), whereas *Igf1r* fluorescence was increased in Se FBOs ([Supplementary Fig. 4D](#)). Further analysis revealed a significantly higher fraction of *Igf1r⁺Nucb2⁺* FBOs ([Supplementary Fig. 4E](#)) and a lower fraction of *Vegfa⁺Nucb2⁺* ECs ([Supplementary Fig. 4F](#)) in Se BAT ([Fig. 7B](#)), confirming the ligand–receptor switch identified *in silico*.

To assess human relevance, we re-analyzed the public visceral adipose snRNA-seq data set GSE295708[38]. After replicating the original cell-type annotation ([Fig. 7C–D](#)), we compared EC and adipocyte subpopulations between obese and weight-loss individuals. ECs from weight-loss subjects exhibited a significant reduction in VEGF-pathway activity (AddModuleScore, $p < 0.0001$, [Fig. 7E](#)), paralleling the Je mouse signature. *NUCB2* expression was up-regulated in nearly all adipocyte sub-clusters after weight loss ([Fig. 7F–H](#)), mirroring the Se-enriched *Nucb2* expression observed in mice. These cross-species findings

underscore the translational relevance of *Nucb2* identified in our model.

Fig. 7 Cross-species validation of FBO/EC markers and pathway activity after weight-loss surgery. **(A, B)** Immunofluorescence staining of brown adipose tissue before and after surgery: NUCB2 and IGF1R co-localization in FBO (**A**); EMCN and IGF1R co-localization in EC (**B**); **(C – H)** Human adipose tissue snRNA-seq: UMAP of nuclei colored by major cell type (**C**); ADIPOQ expression overlaid on the UMAP (**D**); VEGF-pathway activity scores: Obese vs Weight-loss (**E**); NUCB2 expression: Obese vs Weight-loss (**F**); UMAP of adipocyte subclusters (**G**); NUCB2 levels across adipocyte subclusters: Obese vs Weight-loss (**H**). 

**** $p < 0.0001$ using the two-tailed unpaired t-test

Discussion

Our study provides valuable insights into the dynamic remodeling of brown and beige adipose tissue following bariatric surgery, elucidating the cellular and molecular mechanisms underlying post-surgical metabolic adaptations. We show that surgery markedly alters the adipose microenvironment, reducing the adipocyte (AP) pool and expanding the fibroblastoid (FBO) compartment in both brown and beige depots. This shift is accompanied by enhanced IGF1-IGF1R signaling, indicating that the IGF1 pathway is a key facilitator of adipose fibrogenesis after bariatric intervention.

We identify the BAT AP6 sub-cluster as a central contributor to this process. AP6 is characterized by high expression of *Zbtb16* and *Fkbp5*, two transcriptional regulators previously implicated in tissue fibrosis[31, 33]. Within the 11-gene AP6→FBO transition signature, *Nucb2* emerges as a specific AP6 marker. Its protein product, nesfatin-1, is markedly elevated in human cystic fibrosis and correlates inversely with fat mass[39, 40], implying a direct link between *Nucb2*/nesfatin-1 and fibrotic remodelling. Three additional

transition genes—*Ano1/Tmem16a*, *Iqgap2* and *St8sia6*—have also been associated with either glucose metabolism or organ fibrosis[41-43].

Co-expression analysis further revealed that *Nucb2* and the other transition genes track closely with *Igflr* in BAT FBOs. IGF1-IGF1R signaling is a well-characterized pro-fibrotic axis in liver and lung[44, 45]; our data now extend this pathway to adipose tissue and position *Nucb2* as a potential co-activator of IGF1-driven fibrosis. Importantly, the pro-fibrotic role of *Nucb2* appears to be tissue-specific: in pulmonary fibrosis nesfatin-1 is reportedly protective via AMPK α -mediated suppression of TGF- β 1/Smad signaling[46]. Thus, the *Nucb2-Igfl* circuit we uncover in adipose tissue represents a context-dependent regulatory module that may be exploited to limit fibrotic expansion after bariatric surgery.

Several limitations inherent to snRNA-seq should be noted[47]. First, nuclear transcripts lack the bulk of cytoplasmic mRNA, leading to under-representation of secreted factors and other cytosolic RNAs. Second, the lower RNA content per nucleus increases dropout rates and hampers detection of low-abundance genes. Third, many immune and neuronal subsets are annotated on the basis of cytoplasmic markers; their absence can misclassify or mask rare populations. Finally, mechanical isolation of nuclei can induce immediate-early gene expression and residual cytoplasmic contamination can skew transcript counts.

Beyond these technical considerations, this study has two additional limitations. First, the limited sample size renders the findings primarily descriptive and hypothesis-generating; definitive lineage inference will require fate-mapping or RNA-velocity analyses in larger cohorts with additional biological replicates. Second, although we nominate 11 candidate regulators co-expressed with IGF1R and potentially cooperating with IGF1 signaling during the AP6→FBO transition, this set is sensitive to analytical parameterization and remains provisional pending targeted functional validation.

In conclusion, we define an AP6→FBO transition programme—anchored by *Nucb2* and IGF1 signaling—that drives fibrogenic remodelling of brown and beige adipose tissue after bariatric surgery. Monitoring this gene signature in small needle biopsies (qPCR or

RNA-scope) could provide clinicians with an objective metric to assess operative outcome and to identify patients who might benefit from adjunct anti-fibrotic or pro-adipogenic therapy.

Acknowledgements

The author would like to thank the following personnel and suppliers whom provided technical services: Dr. Yuxiang Zhao from Biotrans Technology Co., LTD provided technical support for single-nucleus bioinformatics analysis, and Dr. Jihong Yang from BoYu Intelligent Health Innovation Laboratory have provided a lot of assistance for this study.

Authors contributions

RBL and WX directed the study, were responsible for study design, interpretation of data, and overall project management, and revised the manuscript and approved the final version to be published. YXYW, ZHG and YL performed the animal experiments, WW wrote the first draft of the manuscript, and reviewed and edited the final manuscript. All authors have approved the final version to be published. RBL is responsible for the integrity of the work as a whole.

Funding

The work was funded by the Natural Science Foundation of Inner Mongolia Autonomous Region of China (NO.2023MS08048)

Data Availability

The raw FASTQ files and processed snRNA-seq data in this study can be obtained from Gene Expression Omnibus (GEO) with an accession number of GSE307599. The source codes utilized for generating the results in this study can be archived in a GitHub repository at https://github.com/StephenCLab/Adipocyte_SCAna.

Ethics approval and consent to participate

Animal ethics approval was granted by the Medical Ethics Committee of the First Affiliated Hospital of Baotou Medical College, Inner Mongolia University of Science and Technology, under approval number 2024D027.

Consent for publication

All authors have given consent to publish.

Competing interests

The authors declare that they have no competing interests.

References

1. Rubino F, Cummings DE, Eckel RH, Cohen RV, Wilding JPH, Brown WA, Stanford FC, Batterham RL, Farooqi IS, Farpour-Lambert NJ *et al*: **Definition and diagnostic criteria of clinical obesity.** *The lancet Diabetes & endocrinology* 2025, **13**(3):221-262.[https://doi.org/10.1016/s2213-8587\(24\)00316-4](https://doi.org/10.1016/s2213-8587(24)00316-4)
2. Lin X, Xu Y, Xu J, Pan X, Song X, Shan L, Zhao Y, Shan P-F: **Global burden of noncommunicable disease attributable to high body mass index in 195 countries and territories, 1990–2017.** *Endocrine* 2020, **69**(2):310-320.<https://doi.org/10.1007/s12020-020-02352-y>
3. Haeuser E, Serfes AL, Cork MA, Yang M, Abbastabar H,

- Abhilash ES, Adabi M, Adebayo OM, Adekanmbi V, Adeyinka DA *et al: Mapping age- and sex-specific HIV prevalence in adults in sub-Saharan Africa, 2000–2018. BMC medicine* 2022, **20**(1):488.<https://doi.org/10.1186/s12916-022-02639-z>
4. Xie J, Wang Y: **Multidisciplinary combined treatment based on bariatric surgery for metabolic syndrome: a review article.** *International Journal of Surgery* 2024, **110**(6):3666-3679.<https://doi.org/10.1097/j.s.0000000000001320>
5. Akalestou E, Miras AD, Rutter GA, le Roux CW: **Mechanisms of Weight Loss After Obesity Surgery.** *Endocrine reviews* 2022, **43**(1):19-34.<https://doi.org/10.1210/endrev/bnab022>
6. Ospina Jaramillo A, Riscanevo Bobadilla AC, Espinosa MO, Valencia A, Jiménez H, Montilla M, Bastidas M: **Clinical outcomes and complications of single anastomosis duodenal-ileal bypass with sleeve gastrectomy: A 2-year follow-up study in Bogotá, Colombia.** *World journal of clinical cases* 2023, **11**(21):5035-5046.<https://doi.org/10.12998/wjcc.v11.i21.5035>

7. Bramante C, Wise E, Chaudhry Z: **Care of the Patient After Metabolic and Bariatric Surgery.** *Annals of internal medicine* 2022,
175(5):ITC65-ITC80.<https://doi.org/10.7326/aitc202205170>
8. Mathurin P, Hollebecque A, Arnalsteen L, Buob D, Leteurtre E, Caiazzo R, Pigeyre M, Verkindt H, Dharancy S, Louvet A *et al:* **Prospective Study of the Long-Term Effects of Bariatric Surgery on Liver Injury in Patients Without Advanced Disease.** *Gastroenterology* 2009,
137(2):532-540.<https://doi.org/10.1053/j.gastro.2009.04.052>
9. Hagberg CE, Spalding KL: **White adipocyte dysfunction and obesity-associated pathologies in humans.** *Nature Reviews Molecular Cell Biology* 2023,
25(4):270-289.<https://doi.org/10.1038/s41580-023-00680-1>
10. Kahn CR, Wang G, Lee KY: **Altered adipose tissue and adipocyte function in the pathogenesis of metabolic syndrome.** *The Journal of clinical investigation* 2019,
129(10):3990-4000.<https://doi.org/10.1172/jci129187>
11. Azzu V, Vacca M, Virtue S, Allison M, Vidal-Puig A: **Adipose**

Tissue-Liver Cross Talk in the Control of Whole-Body Metabolism: Implications in Nonalcoholic Fatty Liver Disease. *Gastroenterology* 2020,
158(7):1899-1912.<https://doi.org/10.1053/j.gastro.2019.12.054>

12. Cypess AM, Ingelfinger JR: **Reassessing Human Adipose Tissue.** *New England Journal of Medicine* 2022,
386(8):768-779.<https://doi.org/10.1056/NEJMra2032804>
13. Chouchani ET, Kajimura S: **Metabolic adaptation and maladaptation in adipose tissue.** *Nature metabolism* 2019,
1(2):189-200.<https://doi.org/10.1038/s42255-018-0021-8>
14. Reverte-Salisa L, Siddig S, Hildebrand S, Yao X, Zurkovic J, Jaeckstein MY, Heeren J, Lezoualc'h F, Krahmer N, Pfeifer A: **EPAC1 enhances brown fat growth and beige adipogenesis.** *Nature cell biology* 2024,
26(1):113-123.<https://doi.org/10.1038/s41556-023-01311-9>
15. Wang H, Yu L, Wang Je, Zhang Y, Xu M, Lv C, Cui B, Yuan M, Zhang Y, Yan Y *et al:* **SLC35D3 promotes white adipose tissue browning to ameliorate obesity by NOTCH signaling.** *Nature communications* 2023,

- 14(1):7643.<https://doi.org/10.1038/s41467-023-43418-5>
16. Hinte LC, Castellano-Castillo D, Ghosh A, Melrose K, Gasser E, Noé F, Massier L, Dong H, Sun W, Hoffmann A *et al*: **Adipose tissue retains an epigenetic memory of obesity after weight loss.** *Nature* 2024, **636**(8042):457-465.<https://doi.org/10.1038/s41586-024-08165-7>
17. Divoux A, Tordjman J, Lacasa D, Veyrie N, Hugol D, Aissat A, Basdevant A, Guerre-Millo M, Poitou C, Zucker J-D *et al*: **Fibrosis in Human Adipose Tissue: Composition, Distribution, and Link With Lipid Metabolism and Fat Mass Loss.** *Diabetes* 2010, **59**(11):2817-2825.<https://doi.org/10.2337/db10-0585>
18. Abdennour M, Reggio S, Le Naour G, Liu Y, Poitou C, Aron-Wisnewsky J, Charlotte F, Bouillot J-L, Torcivia A, Sasso M *et al*: **Association of Adipose Tissue and Liver Fibrosis With Tissue Stiffness in Morbid Obesity: Links With Diabetes and BMI Loss After Gastric Bypass.** *The Journal of Clinical Endocrinology & Metabolism* 2014, **99**(3):898-907.<https://doi.org/10.1210/jc.2013-3253>
19. Bel Lassen P, Charlotte F, Liu Y, Bedossa P, Le Naour G,

Tordjman J, Poitou C, Bouillot J-L, Genser L, Zucker J-D *et al*:

**The FAT Score, a Fibrosis Score of Adipose Tissue:
Predicting Weight-Loss Outcome After Gastric Bypass.** *The
Journal of Clinical Endocrinology & Metabolism* 2017,
102(7):2443-2453. <https://doi.org/10.1210/jc.2017-001>

38

20. Emont MP, Jacobs C, Essene AL, Pant D, Tenen D, Colleluori G, Di Vincenzo A, Jørgensen AM, Dashti H, Stefek A *et al*: **A single-cell atlas of human and mouse white adipose tissue.** *Nature* 2022,
603(7903):926-933. <https://doi.org/10.1038/s41586-022-04518-2>
21. Sárvári AK, Van Hauwaert EL, Markussen LK, Gammelmark E, Marcher A-B, Ebbesen MF, Nielsen R, Brewer JR, Madsen JGS, Mandrup S: **Plasticity of Epididymal Adipose Tissue in Response to Diet-Induced Obesity at Single-Nucleus Resolution.** *Cell metabolism* 2021,
33(2):437-453.e435. <https://doi.org/10.1016/j.cmet.2020.12.004>
22. Massier L, Jalkanen J, Elmastas M, Zhong J, Wang T, Nono Nankam PA, Frendo-Cumbo S, Bäckdahl J, Subramanian N, Sekine T *et al*: **An integrated single cell and spatial**

- transcriptomic map of human white adipose tissue.** *Nature communications* 2023,
14(1):1438. <https://doi.org/10.1038/s41467-023-36983-2>
23. Stuart T, Butler A, Hoffman P, Hafemeister C, Papalexi E, Mauck WM, Hao Y, Stoeckius M, Smibert P, Satija R: **Comprehensive Integration of Single-Cell Data.** *Cell* 2019, **177(7):1888-1902.e1821.** <https://doi.org/10.1016/j.cell.2019.05.031>
24. Dong H, Sun W, Shen Y, Baláz M, Balázová L, Ding L, Löffler M, Hamilton B, Klöting N, Blüher M *et al*: **Identification of a regulatory pathway inhibiting adipogenesis via RSPO2.** *Nature metabolism* 2022, **4(1):90-105.** <https://doi.org/10.1038/s42255-021-00509-1>
25. Sanz I, Wei C, Jenks SA, Cashman KS, Tipton C, Woodruff MC, Hom J, Lee FE-H: **Challenges and Opportunities for Consistent Classification of Human B Cell and Plasma Cell Populations.** *Frontiers in immunology* 2019, **10:2458.** <https://doi.org/10.3389/fimmu.2019.02458>
26. Humphreys DT, Lewis A, Pan - Castillo B, Berti G, Mein C, Wozniak E, Gordon H, Gadrok R, Minicozzi A, ChinAleong J

- et al: Single cell sequencing data identify distinct B cell and fibroblast populations in stricturing Crohn's disease.*
Journal of cellular and molecular medicine 2024,
28(9):e18344.<https://doi.org/10.1111/jcmm.18344>
27. Sinha D, Kumar A, Kumar H, Bandyopadhyay S, Sengupta D: **dropClust: efficient clustering of ultra-large scRNA-seq data.** *Nucleic acids research* 2018,
46(6):e36-e36.<https://doi.org/10.1093/nar/gky007>
28. Skelly DA, Squiers GT, McLellan MA, Bolisetty MT, Robson P, Rosenthal NA, Pinto AR: **Single-Cell Transcriptional Profiling Reveals Cellular Diversity and Intercommunication in the Mouse Heart.** *Cell reports* 2018,
22(3):600-610.<https://doi.org/10.1016/j.celrep.2017.12.072>
29. Guerrero-Juarez CF, Dedhia PH, Jin S, Ruiz-Vega R, Ma D, Liu Y, Yamaga K, Shestova O, Gay DL, Yang Z *et al:* **Single-cell analysis reveals fibroblast heterogeneity and myeloid-derived adipocyte progenitors in murine skin wounds.** *Nature communications* 2019,
10(1):650.<https://doi.org/10.1038/s41467-018-08247-x>
30. Hu C, Li T, Xu Y, Zhang X, Li F, Bai J, Chen J, Jiang W, Yang K, Ou Q *et al:* **CellMarker 2.0: an updated database of**

manually curated cell markers in human/mouse and web tools based on scRNA-seq data. *Nucleic acids research* 2023, **51**(D1):D870-D876. <https://doi.org/10.1093/nar/gkac94>

7

31. Zhang H, Qiu J, Zhao Q, Zhang Y, Zheng H, Dou Z, Yan Y: **Tanshinone IIA alleviates bleomycin-induced pulmonary fibrosis by inhibiting Zbtb16.** *Pulmonary pharmacology & therapeutics* 2024, **84**:102285. <https://doi.org/10.1016/j.pupt.2024.102285>
32. ŠEda O, ŠEdová L, VČEĽÁK J, VaŇKOVÁ M, LiŠKA F, Bendlová B: **ZBTB16 and Metabolic Syndrome: a Network Perspective.** *Physiological research* 2017, **66**(Suppl 3):S357-S365. <https://doi.org/10.33549/physiolres.933730>
33. Liu X, Zhang J, Liang Y, Chen X, Xu S, Lin S, Dai Y, Chen X, Zhou Y, Bai Y *et al*: **tiRNA - Gly - GCC - 002 promotes epithelial - mesenchymal transition and fibrosis in lupus nephritis via FKBP5 - mediated activation of Smad.** *British journal of pharmacology* 2024, **182**(3):616-632. <https://doi.org/10.1111/bph.17364>
34. Angelone T, Rocca C, Pasqua T: **Nesfatin-1 in cardiovascular**

- orchestration: From bench to bedside.** *Pharmacological research* 2020,
156:104766.<https://doi.org/10.1016/j.phrs.2020.104766>
35. Wang Y, Li Z, Zhang X, Xiang X, Li Y, Mulholland MW, Zhang W: **Nesfatin-1 promotes brown adipocyte phenotype.** *Scientific reports* 2016,
6(1):34747.<https://doi.org/10.1038/srep34747>
36. He Y, Zhang C, Wu S, Li K, Zhang S, Tian M, Chen C, Liu D, Yang G, Li L *et al*: **Central NUCB2/nesfatin-1 signaling ameliorates liver steatosis through suppression of endoplasmic reticulum stress in the hypothalamus.** *Metabolism: clinical and experimental* 2025,
162:156046.<https://doi.org/10.1016/j.metabol.2024.156046>
37. Geng S, Yang S, Tang X, Xue S, Li K, Liu D, Chen C, Zhu Z, Zheng H, Wang Y *et al*: **Intestinal NUCB2/nesfatin-1 regulates hepatic glucose production via the MC4R-cAMP-GLP-1 pathway.** *The EMBO journal* 2024,
44(1):54-74.<https://doi.org/10.1038/s44318-024-00300-4>
38. Miranda AMA, McAllan L, Mazzei G, Andrew I, Davies I,

- Ertugrul M, Kenkre J, Kudo H, Carrelha J, Patel B *et al*:
Selective remodelling of the adipose niche in obesity and weight loss. *Nature* 2025,
644(8077):769-779.<https://doi.org/10.1038/s41586-025-09233-2>
39. Mori M, Ohshima K, Okada S, Miura A, Tagaya Y:
Nucleobindin-2 Is a Positive Modulator of EGF-Dependent Signals Leading to Enhancement of Cell Growth and Suppression of Adipocyte Differentiation. *Endocrinology* 2012,
153(7):3308-3319.<https://doi.org/10.1210/en.2011-215-4>
40. Cohen RI, Ginsberg N, Tsang D, Wann LC, Ye X, Liu SF:
Association of Nesfatin-1 and Fat Mass in Cystic Fibrosis. *Respiration; international review of thoracic diseases* 2013,
86(4):312-317.<https://doi.org/10.1159/000345375>
41. Ji J-L, Li J-Y, Liang J-X, Zhou Y, Liu C-C, Zhang Y, Zhang A-Q, Liu H, Ma R-X, Li Z-L: **Tubular TMEM16A promotes tubulointerstitial fibrosis by suppressing PGC-1 α -mediated mitochondrial homeostasis in diabetic kidney disease.** *Cellular and Molecular Life Sciences* 2023,
80(12):347.<https://doi.org/10.1007/s00018-023-05000-8>

6

42. Sen A, Youssef S, Wendt K, Anakk S: **Depletion of IQ motif-containing GTPase activating protein 2 (IQGAP2) reduces hepatic glycogen and impairs insulin signaling.** *The Journal of biological chemistry* 2023, **299**(11):105322.<https://doi.org/10.1016/j.jbc.2023.105322>
43. Takashima S, Ishida H-k, Inazu T, Ando T, Ishida H, Kiso M, Tsuji S, Tsujimoto M: **Molecular Cloning and Expression of a Sixth Type of α2,8-Sialyltransferase (ST8Sia VI) That Sialylates O-Glycans.** *The Journal of biological chemistry* 2002, **277**(27):24030-24038.<https://doi.org/10.1074/jbc.M112367200>
44. Svegliati-Baroni G, Ridolfi F, Di Sario A, Casini A, Marucci L, Gaggiotti G, Orlandoni P, Macarri G, Perego L, Benedetti A *et al*: **Insulin and Insulin-Like Growth Factor-1 Stimulate Proliferation and Type I Collagen Accumulation by Human Hepatic Stellate Cells: Differential Effects on Signal Transduction Pathways.** *Hepatology* 1999, **29**(6):1743-1751.<https://doi.org/10.1002/hep.51029063>

2

45. Hung CF, Rohani MG, Lee S-s, Chen P, Schnapp LM: **Role of IGF-1 pathway in lung fibroblast activation.** *Respiratory research* 2013, **14**(1):102.<https://doi.org/10.1186/1465-9921-14-102>
46. Zhang R, Liang H, Liu G, Jiang W, Tang Z, Fan Q, Nie Z, Hu H, Kang G, Xie S: **Nesfatin-1, a novel energy-regulating peptide, alleviates pulmonary fibrosis by blocking TGF-β1/Smad pathway in an AMPKα-dependent manner.** *International immunopharmacology* 2023, **120**:110369.<https://doi.org/10.1016/j.intimp.2023.110369>
47. Kim N, Kang H, Jo A, Yoo S-A, Lee H-O: **Perspectives on single-nucleus RNA sequencing in different cell types and tissues.** *Journal of pathology and translational medicine* 2023, **57**(1):52-59.<https://doi.org/10.4132/jptm.2022.12.19>